JOURNAL OF MATERIALS SCIENCE **34** (1999) 4001–4010

Nonlinear electric-mechanical behavior of a soft PZT-51 ferroelectric ceramic

DAINING FANG, CHANGQING LI
Department of Engineering Mechanics, Tsinghua University, Beijing 100084, People's Republic of China
E-mail: fangdn@mail.tsinghua.edu.cu

In this investigation, the electric-mechanical response of a PZT ferroelectric ceramic subjected to the combined electric-mechanical loads was experimentally observed. The effect of different compressive stress levels on the electromechanical response was examined. The stress-strain relationship was also measured. The ceramic sample was isolated from the test frame and the high voltage arcing were prevented effectively in the setup which promotes the precise measurement and makes the systemic experimental results available. With a high voltage amplifier and a servo-hydraulic test frame, the butterfly shaped strain vs. electric field curves and the electric displacement vs. electric field hysteresis loops of a soft PZT ceramic at different compressive stress levels were measured. The results show that the electric-mechanical coupled properties of the PZT ceramic are the function of the compressive stress. The switching criteria are given to account for the experimental results and to analyze the nonlinear electric-mechanical behavior relative to the domain switching process in this paper.

1. Introduction

Lead Zirconate Titanate (PZT), with large piezoelectric coefficient, large dielectric coefficient and quick time response, was found to be excellent piezoelectric ceramics based on ferroelectric crystals in 1954. Due to their intrinsic electromechanical coupling properties, PZT ceramics have widely been used as electromechanical sensors, transducers and actuators [1–3]. Jaffe *et al.* studied the piezoelectric properties of PZT ceramics systemically first [4]. By modifying PZT compositions with different additives such as lanthanum, specific properties can be tailored to suit specific materials applications. The PZT family can be roughly classified into two groups: "hard" and "soft". The hard materials, such as PZT-81, typically can withstand high electric fields and mechanical stress. However, they offer smaller generated strains. On the other hand, soft materials, such as PZT-51, can offer higher sensitivity and piezoelectric activity.

PZT ceramic deforms under an applied electric field. Piezoelectricity is a first-order phenomenon of electromechanical coupling, exhibiting a nearly linear relationship between induced strain and the applied electric field. However, as the field becomes larger, the strain deviates from linearity, and significant hysteresis appears because of the domain switching. The hysteresis limits the application of the PZT ceramics, especially under the large applied electric or stress field. The study on the hysteresis can exhume the potential application of the materials.

PZT ceramics are susceptible to brittle fracture that can lead to catastrophic failure. Therefore, it is important for people to understand the deformation and fracture behaviors of PZT under coupled electromechanical fields [5]. One way to accomplish this is to resort to well-established linear elastic fracture mechanics [6–10]. On the other hand, a better understanding of the fracture behavior in PZT ceramics was obtained on the base of the domain switching mechanisms and related theory of nonlinear fracture mechanics [11, 12]. The crack tip stress fields are singular so that the induced strain fields near the crack tip are nonlinear. This implies that the structure reliability concerns of electromechanical devices call for a better understanding of nonlinear constitutive laws of ferroelectric ceramics as well as related domain-switching criteria. Although there have had no reasonable theoretical constitutive laws so far, the experimental study becomes very important. The relationship between stress and strain in PZT ceramics subjected to the uniaxial stress field was investigated by Cao and Evans [13] as well as Schaufele and Hardltl [14]. The hysteresis behavior of a lead lanthanum zirconate titanate (PLZT) ceramic subjected to electromechanical coupling loads was studied as well [15, 16]. In this investigation, the electric-mechanical response of a soft PZT-51 ceramic under combined electric-mechanical loads was experimentally observed. The effect of different compressive stress levels on the electromechanical response was examined. With a high voltage amplifier and a servo-hydraulic test frame, the strain vs. electric field curves and electric displacement vs. electric field hysteresis loops of a soft PZT ceramic at different compressive stress levels were measured. The results show that the

TABLE I Properties of the soft PZT-51 ceramic

Physical properties	Published	Measured
Piezoelectric coefficient d_{333} (10^{-12} C/N)	>600	1520
Piezoelectric coefficient d_{311} (10^{-12} C/N)	>186	570
Dielectric permittivity ε_{33} ($\varepsilon_r = \varepsilon/\varepsilon_0$, $\varepsilon_0 = 8.85 \times 10^{-12}$ F/m)	2200 ε_0	11300 ε_0
Elastic modulus Y_{3333} (m^2/N)	10^{-12}	3.03×10^{-11}
Elastic modulus Y_{3311} (m^2/N)	10^{-12}	2.9×10^{-11}
Remnant polarization P^r (C/m^2)		0.1938
Coercive electric E_c (MV/m)		0.676

electric-mechanical properties of the PZT ceramic are the function of the compressive stress. The switching criteria are given to account for the experimental results and to analyze the nonlinear electric-mechanical behavior relative to the domain switching process in this paper.

2. Experimental

The material chosen for this investigation is a typical soft PZT-51 that has been used widely in modern industry, such as ultrasonic testing, actuators and sensors because it has very large piezoelectric coefficients and dielectric permittivity. Each grain of the ceramic is a single crystal with a tetragonal perovskite structure at the room temperature. The published physical properties and the measured physical properties of the soft PZT-51 ceramic are listed in Table I. The specimens, with nominal dimensions $10 \times 10 \times 16$ mm, were cut from bulk ferroelectrics, and all faces were polished. The upper and bottom faces of the specimens with an area of 10×10 mm were electroded with sputtered Ag. The hysteresis loops of strain vs. electric field as well as electric field vs. electric displacement are measured by a modified Sawyer-Tower circuit as demonstrated in Fig. 1. A servo-hydraulic loading fixture is set up for applying stress field. A silicon oil bath is mounted on the loading fixture to prevent high voltage arcing. When applied combined electric-mechanical loads, unpolarized samples are subjected to cyclic electric field under different constant compressive stresses. When applied only a mechanical load, the stress field is applied to a polarized sample.

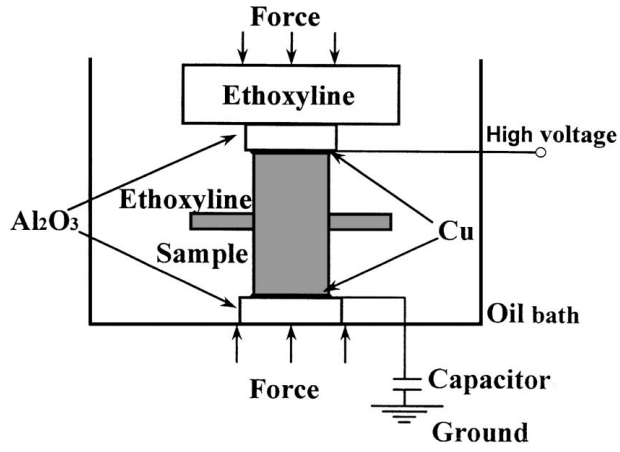

Figure 2 Schematic of the electric-mechanical loading system.

As showing in Fig. 2, the sample is isolated from the fixture by two aluminum blocks and one ethoxyline block. The high voltage arcing is prevented effectively by the silicon oil bath and a ringed ethoxyline block in the middle of the sample. For protecting the strain gauges from the high voltage arcing, they must be bonded to the area near the ground electrode and covered by a special isolated-glue. To avoid the bending stress and the inhomogeneous distribution of the stress, the upper and bottom faces of both the aluminum blocks and the ethoxyline block are kept parallel (misalignment < 0.01 mm). Besides, one spherical cone is incorporated in the setup. Also to ensure the upper and bottom faces to be parallel to each other, the sample were polished again after two faces were electroded.

A 50 kN load sensor is installed on the test fixture to monitor the force applied to the specimen. The load sensor output is recorded through the A/D circuit connected to the computer. The stress is determined from the force and the cross sectional area of the specimen. Longitudinal and transverse strain gauges are bonded to the center of the area near the ground electrode to

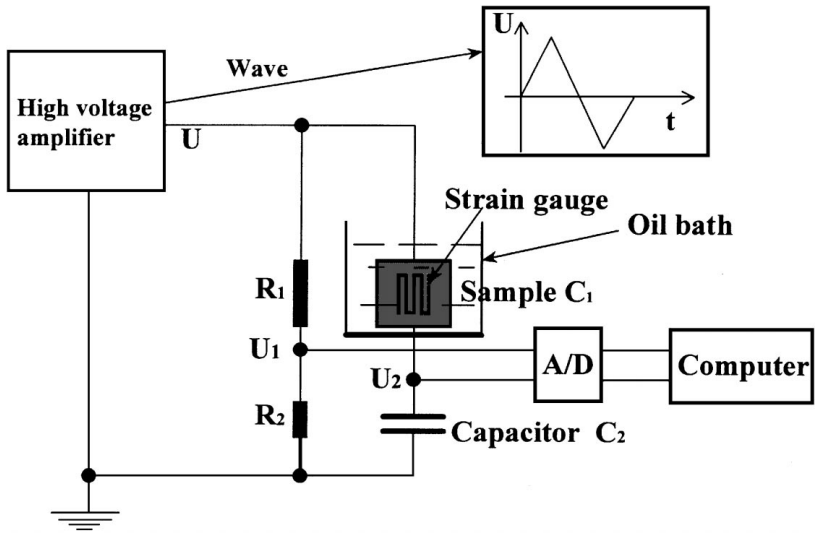

Figure 1 Approach of testing measurements. The electric displacement is monitored by voltage U2 and the electric field is measured by voltage U1.

measure the strain parallel and perpendicular to the polarization direction. The strain gauges are connected to a Wheastone bridge and A/D circuit connected to the computer. The charge per unit area on the electrode is equal to the normal component of the electric displacement. The charge on the electrode is measured by monitoring the voltage of an capacitor (10 μF) connected from the bottom electrode of the specimen to the ground. The voltage of the capacitor is monitored by means of a high input impedance electrometer and the A/D circuit connected to the computer. A high voltage source triangle wave ($\pm$30 kV at from 1 to 0.01 Hz) is connected to the upper electrode of the specimen. A reference signal (1/10000 times the output) is provided by the source. The reference signal is recorded through the A/D circuit connected to the computer, multiplied by 10000 times and divided by the thickness to obtain the applied electric field.

3. Results

3.1. Electric-field vs. electric-displacement hysteresis curve under applied electric field

The cyclic electric field, E_3, is slowly applied to a initially unpolarized sample. Fig. 3a and b show the initial and stable electric-displacement-electric-field curves, respectively. In Fig. 3, D_3 and E_3 refer to the electric displacement and electric field in the direction of x_3 axis, respectively. As shown in Fig. 3a, an initial electric displacement vs. electric field curve is developed at zero stress. As the electric field is increased, the electric displacement increases linearly first. When the electric field reaches a coercive value of 0.67 MV/m, the sample switches to the polarized state and the electric displacement increases nonlinearly. After several cycles, a stable hysteresis loop generates as shown in Fig. 3b and the polarization of the sample occurs at a slight lower electric field than what is required for the first polarization. This is in full agreement with the results given by Lynch [16]. At point A the electric field is zero and the sample has a remanent polarization of -0.194 C/m^2. A positive electric field (opposite to the direction of polarization) is applied to the sample. At point B, the electric field reaches the coercive field of 0.67 MV/m and the direction of polarization of the sample begins to switch. At point C, the polarization is almost aligned with the positive electric field. The electric field is reduced to zero at point D and the remanent polarization is 0.194 C/m^2. Then a negative electric field (opposite to the present direction of the polarization) is applied to the sample and the electric displacement reduces. At point E the electric field reaches the coercive field of -0.67 MV/m and the polarization starts to switch again. At point F the polarization is aligned with the present electric field. Finally, the electric field is reduced to zero and the state of the sample returns to that of point A.

As the sample is in the polarized states of point A and point D, the electric displacement is linearly proportional to the small change of the electric field. It can be described by the equation:

$$D_3 = \varepsilon_{33} E_3 \tag{1}$$

That is, the slope provides a relative permittivity of $\varepsilon_r = \varepsilon/\varepsilon_0 = 11300$, where the permittivity of the free space is $\varepsilon_0 = 8.85 \times 10^{-12}$ F/m.

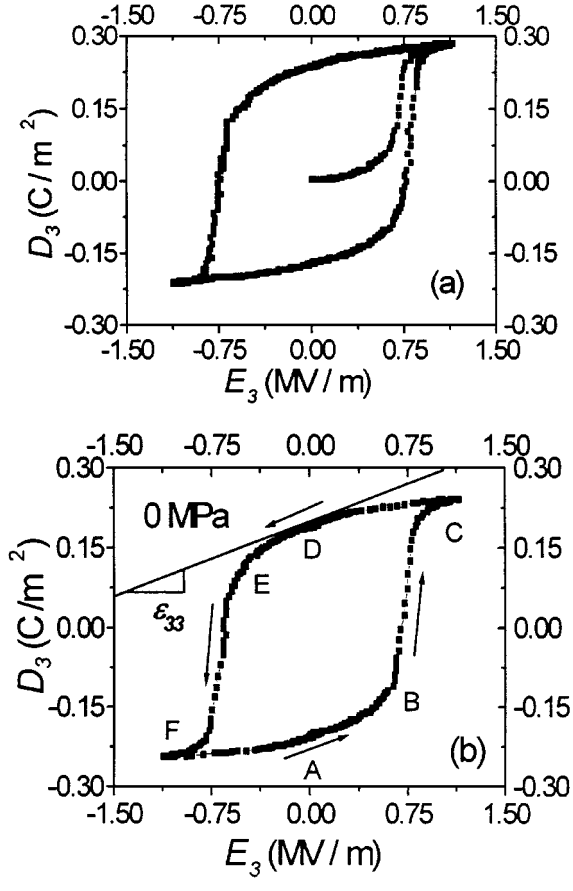

Figure 3 (a) Initial electric field vs. electric displacement hysteresis loop; and (b) stable electric field vs. electric displacement hysteresis loop.

3.2. Strain vs. electric-field hysteresis curve under applied electric field

When the electric field vs. electric displacement hysteresis is developed, the longitudinal strain, e_{33}, and the transverse strain, e_{11}, of the sample are simultaneously recorded. It should be pointed out that the ceramic is transversely isotropic. The polarization direction is parallel to x_3 axis. Thus, the direction of x_3 axis is specified as the longitudinal direction and the x_1-x_2 plane is a transverse plane. At the first cycle of the applied electric field, E_3, as demonstrated in Fig. 4a, there is almost no longitudinal strain until the electric field reaches the coercive field and then the polarization begins to switch. After the electric field reduces to zero, it reverses. When the electric field reaches the coercive field, the polarization switches to the current direction of the electric field. After several cycles the stable electric field vs. longitudinal strain curve is developed as illustrated in Fig. 4b. The points of A, B, C, D, E, F in Fig. 4b correspond to the same points in Fig. 3b in the cycle. At point A the electric field is zero and the sample has a remanent longitudinal strain of 0.0027. As the positive electric field (opposite to the direction of polarization) is applied, the

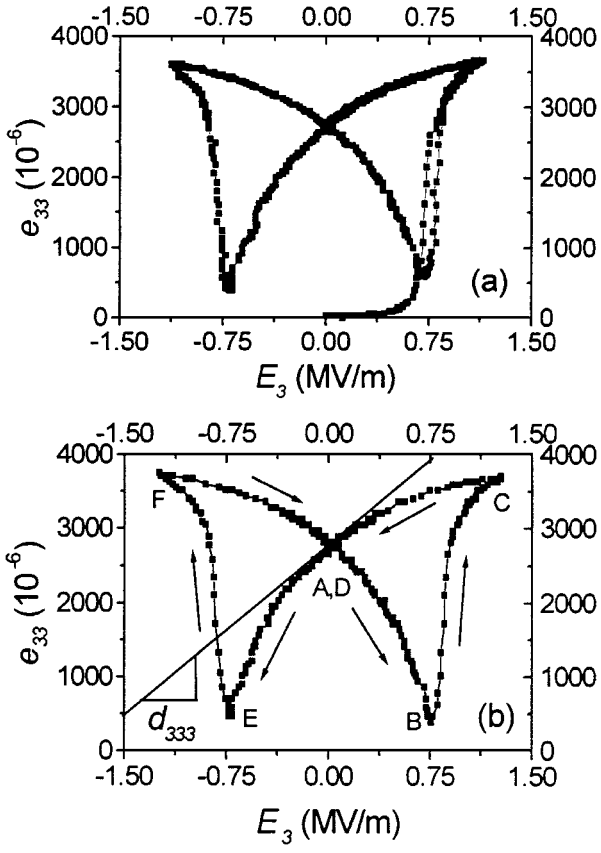

Figure 4 (a) Initial longitudinal strain vs. electric field curve (in first cycle), and (b) stable longitudinal strain vs. electric-field curve (after several cycles).

domains in the sample are constricted by the dielectric effect and the longitudinal strain is reduced. At point B, the electric field reaches the coercive field and the polarization switches to the direction of the electric field. The longitudinal strain increases suddenly. At point C the polarization has switched completely and the strain is linearly proportional to the electric field. As the electric field decreases to zero at point D, the strain returns to that of point A. When a negative electric field (opposite to the current direction of the polarization) is applied to the sample, due to the dielectric effect, the sample is constricted along the direction of the electric field. The longitudinal strain is reduced. At point E the electric reaches the coercive field and the strain increases quickly for the polarization switching. The switch completes at point F. As the electric field decreases to zero, the sample returns to the state of point A and the sequent cycles are followed in the same way. When the electric field is zero (such as at point A and point D), the small change of the longitudinal strain is linearly proportional to the small change of the electric field. This phenomenon can be described by:

$$\Delta e_{33} = d_{333}\Delta E_3 \tag{2}$$

Equation 2 is accurate enough when the ΔE is ranged from -0.25 to 0.25 MV/m. The linear piezoelectric coefficient d_{333} can be gotten from the slope of the typical butterfly shaped longitudinal strain vs. electric field hysteresis curve at point A or point D in Fig. 4b.

The butterfly shaped transverse strain vs. electric field hysteresis loop as demonstrated in Fig. 5 indicates

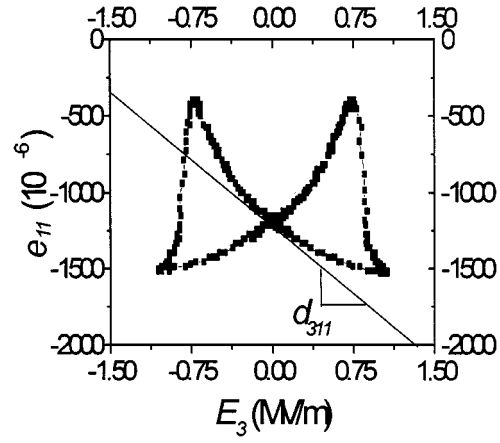

Figure 5 Transverse strain vs. electric field curve without applied stress.

that the transverse strain, e_{11}, is nonlinear to the electric field, E_3, as well and the amplitude is about -0.5 of the longitudinal strain. The linear piezoelectric coefficient, d_{311}, can be gotten too from the slope at the point of zero electric field.

3.3. Stress vs. strain hysteresis curve under applied uniaxial compressive stress

A compressive stress, σ_{33}, is applied to the sample in the polarization direction parallel to x_3 axis. Fig. 6a and b

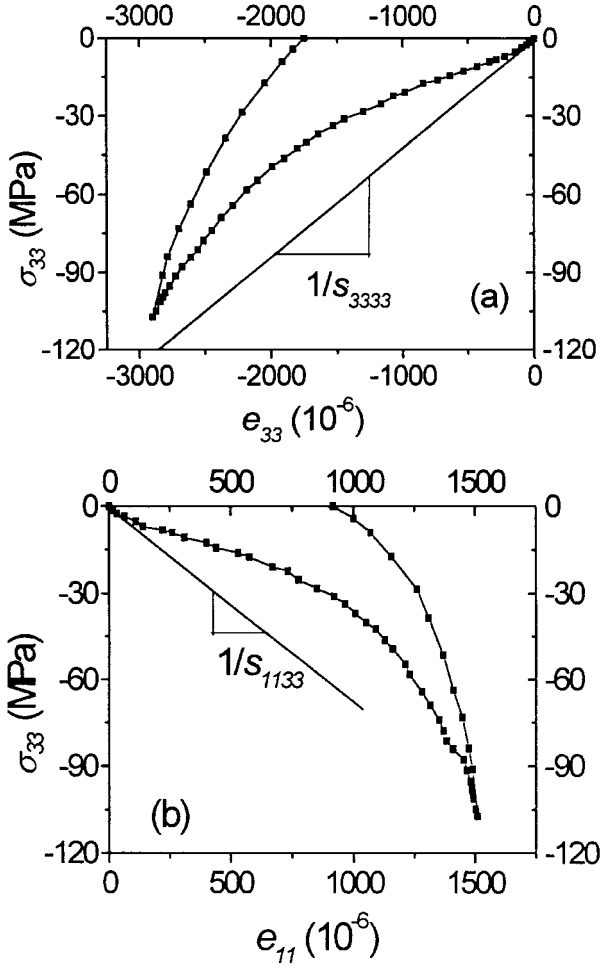

Figure 6 Stress vs. strain curves: (a) longitudinal strain, e_{33}, vs. uniaxial stress, σ_{33}; and (b) transverse strain, e_{11}, vs. uniaxial stress, σ_{33}.

show the longitudinal strain, e_{33}, and transverse strain, e_{11}, vs. electric field, E_3, curves, illustrating that the soft PZT-51 ceramic exhibits linear compressive strain when the uniaxial stress is under 10 MPa. As the stress exceeds 10 MPa, the polarization begins to switch and the sample shows nonlinear deformation. This is in full agreement with the results given by Cao and Evans [13]. After unloading from 110 MPa, the domains partially switch back to their original poling direction and there are a large remanent longitudinal strain, e_{33}, and a remanent transverse strain, e_{11}. The initial slope relating the uniaxial stress to the longitudinal strain is the inverse of the compliance s_{3333} as shown in Fig. 6a. Similarly, the compliance s_{1133} can be obtained from the reverse of the initial slope of the curve in Fig. 6b.

3.4. Electric-displacement vs. electric-field hysteresis curve under combined electric-mechanical loading

In the case of applying combined electric-mechanical loads, a constant compressive stress is imposed in the polarization direction parallel to the x_3 axis while the electric field is cyclically applied. Fig. 7a–h illustrate that electric displacement, D_3, vs. electric field, E_3, hysteresis loops are developed at different constant

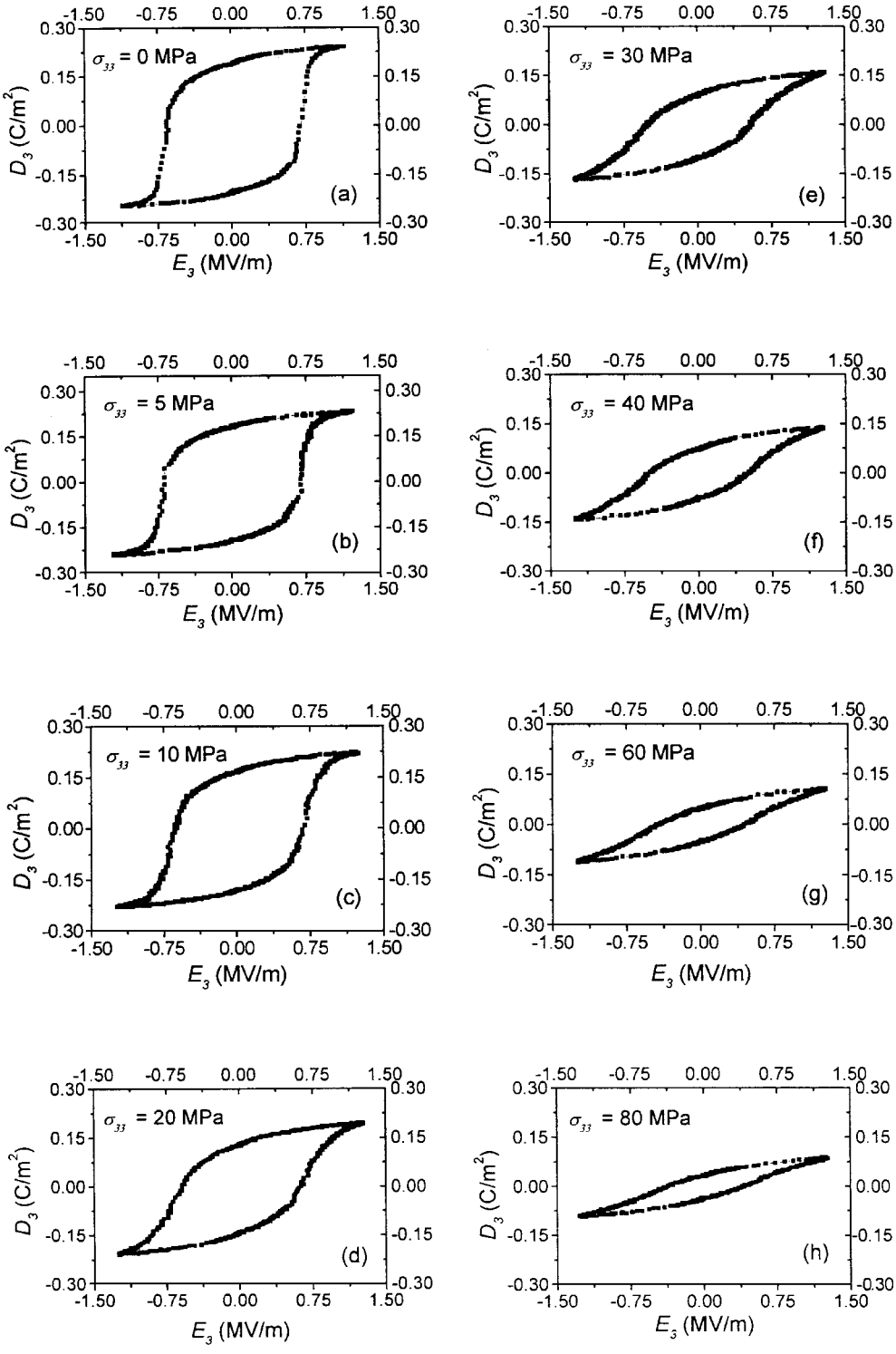

Figure 7 Electric field vs. electric displacement curves at different compressive stress levels: (a) 0.0; (b) 5.0; (c) 10.0; (d) 20.0; (e) 30.0; (f) 40.0; (g) 60.0; and (h) 80.0 MPa.

compressive stress, indicating that there is significant effect of the uniaxial compressive stress on the hysteresis behavior. The resulting hysteresis loops show a steady decrease in both the remanent polarization and the saturation polarization as the compressive stress is increased from 0 to −80 MPa. The slope of the loops at zero electrical field, which can be regarded as the permittivity, decreases when the compressive stress increases. The coercive field decreases linearly too as the uniaxial compressive stress increases. This so-called depolarization phenomenon will be discussed in detail in next section.

3.5. Strain vs. electric field hysteresis curve under combined electric-mechanical loading

The longitudinal strain, e_{33}, vs. electric field, E_3, hysteresis loops in Fig. 8a–h are measured at different constant compressive stresses at the same time when the

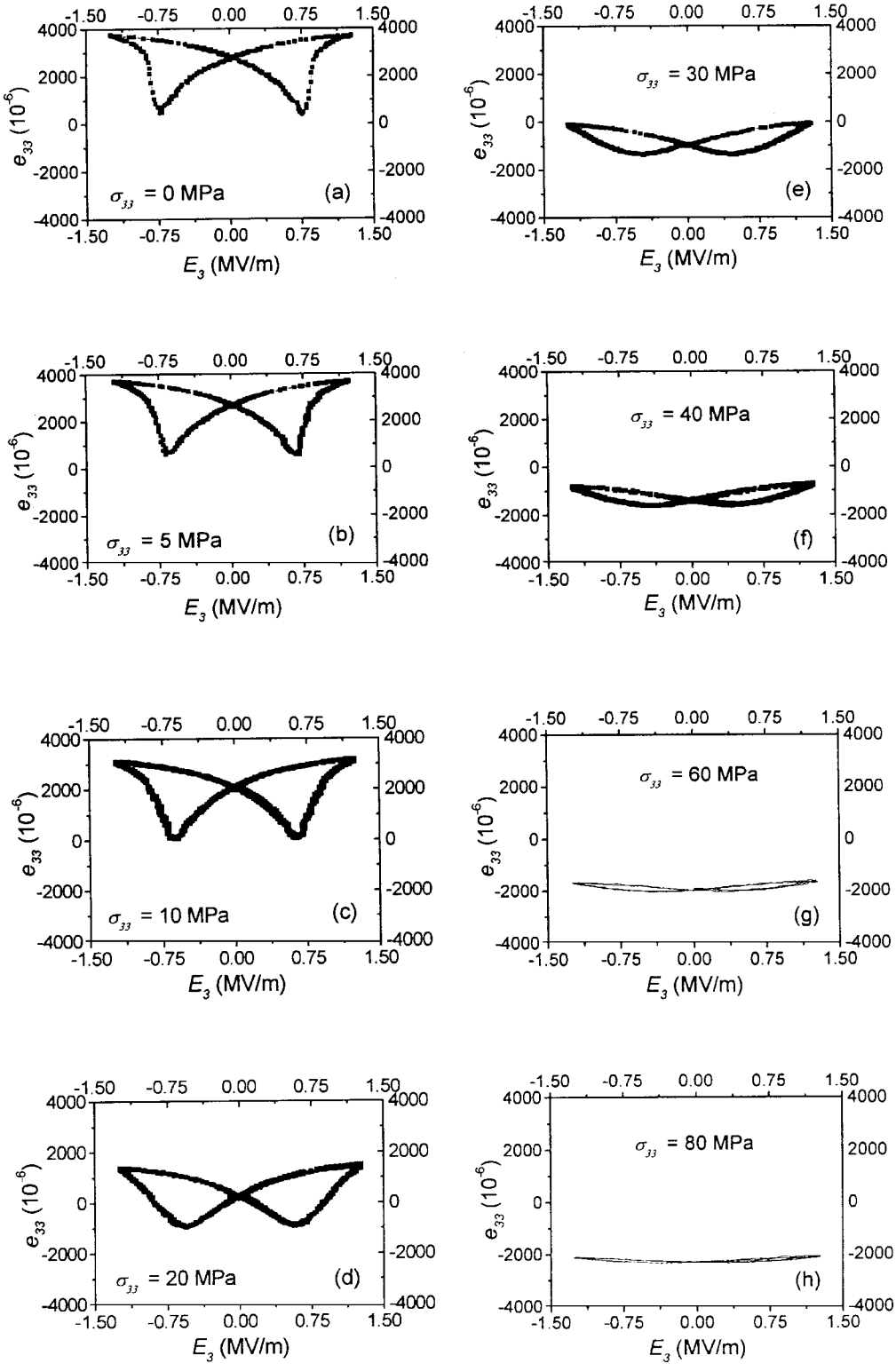

Figure 8 Longitudinal strain vs. electric field curves at different compressive stress levels: (a) 0.0; (b) 5.0; (c) 10.0; (d) 20.0; (e) 30.0; (f) 40.0; (g) 60.0; and (h) 80.0 MPa.

electric displacement vs. electric field hysteresis loops are recorded. The longitudinal strain becomes negative gradually with reference to the unpolarized state when the compressive stress becomes larger. The range of the strain variation becomes smaller and smaller as the compressive stress increases. And the range turns out to be almost zero when the stress goes over −80 MPa which is nearly the coercive stress field. This means that the 180° domains switch more difficult under the greater compressive stress. The slope of the hoops at zero electrical field is not the piezoelectric coefficient but can be considered as the depolarization coefficient under different compressive stress levels. The slope is the function of the stress. The compressive stress acting in conjunction with the electric field induces 90° tetragonal switching. The ceramic remains in this 90° switched state until the electric field is sufficiently high to overcome the applied stress and switch the ceramic back to the polarized state. At a stress level of −80 MPa, the electric field is not able to totally overcome the applied stress and there is very little strain. There is still, however, a substantial component of polarization switching though it is very small. Finally, it must be pointed out that because the domains switch gradually under the electric field larger than the coercive field, the slope also is dependent on the frequency of the applied field.

4. Discussion

Ceramic PZT is produced by high temperature of agglomeration of ferroelectric crystals, such as PbTiO3 and PbZrO3. After the desired crystal structure is gotten by densification and sintering, ceramic PZT is cooled. The single crystal microstructure transforms from a cubic paraelectric phase to a tetragonal ferroelectric phase, when it is cooled through the Curie temperature, T_c. A ferroelectric phase change represents a special class of structure phase transition denoted by the appearance of a spontaneous polarization. Above the Curie temperature the ceramic is cubic and below the Curie temperature it is tetragonal (see Fig. 9). This ABO_3 perovskite structure contains an A^{2+} ion at each corner of the unit cell, an O^{2-} ion at the center of each face, a B^{4+} ion at the center of the unit cell. The cubic

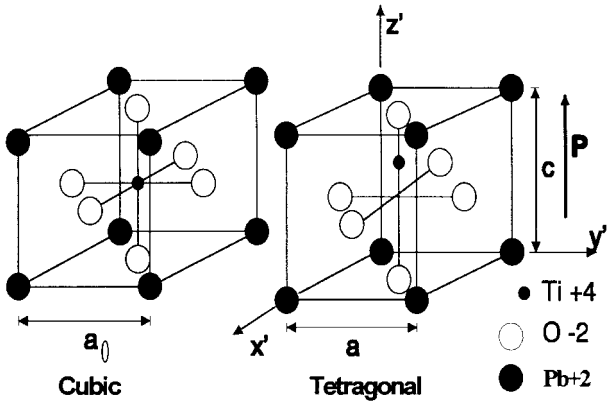

Figure 9 The cubic to tetragonal transition of lead titanate, an ABO_3 perovskite type oxide.

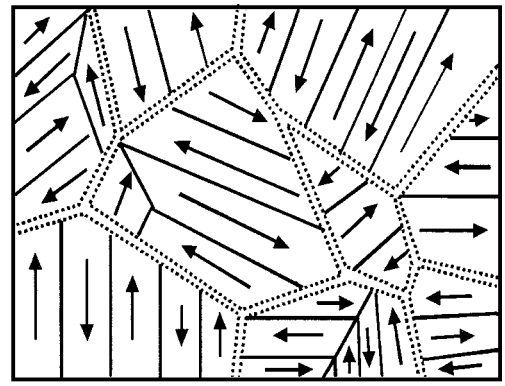

Figure 10 Schematic of the domain and the domain wall.

unit cell has zero ion dipole moment. When the temperature is reduced through the Curie temperature, the unit cell transforms from a cubic state to a tetragonal state and the B^{4+} ion has a displacement relative to the center of the O^{2-} ions. The crystal possesses a spontaneous polarization or electric moment per unit volume due to the displacement.

Below T_c, in the absence of applied field, there are six directions along which a spontaneous polarization can develop. To minimize the depolarizing fields different regions of the crystal polarize in each of these directions, each volume of uniform polarization being called a domain. The interface of two domains with different polarization is such a domain wall as demonstrated in Fig. 10. The resulting domain structure usually results in a near complete compensation of polarization and the crystals consequently exhibit very small piezoelectric effects until they are poled by application of a field.

When the ceramic is subjected to small loads, the polarization of the domain undergoes a reversible change in one of two ways: (1) an applied stress deforms the crystal structure, resulting in a relative displacement of the positive and negative ions; (2) an applied electric field changes the relative displacement of the positive and negative ions, inducing deformation of the crystal structure. These linear effects induce the linear behavior of the crystal. When the applied field excesses the coercive field, domain switching occurs and the central ion is moved to one of the six off-center tetragonal sites. This assigns the direction of the polarization of the domain to that most closely aligned with the electric field (180° domain switching and 90° domain switching). And the applied stress field aligns the direction of the polarization to that most closely perpendicular to the direction of the stress (90° domain switching). Fig. 11 shows the schematic of both 180° and 90° domain switching induced by an applied electric field or a stress field.

The domain switching results in the nonlinear constitutive behaviors of the ceramic. The effect can be estimated by representing each domain as a piezoelectric inclusion in an effective matrix [17–19]. The volume average properties of the inclusions give the macroscopic properties of the ceramic. This micromechanics analysis can be carried out by means of a constitutive model that may predict the mechanical and electrical

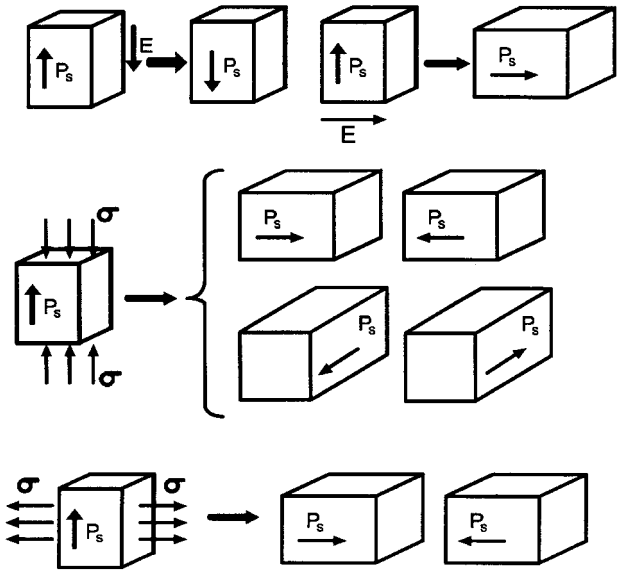

Figure 11 Schematic of the domain switching induced by an applied electrical or mechanical field.

response of the ceramic [17–19]. The domain switching process may account for experimental results. Firstly, when the polarized sample is depoled by compressive stress, the longitudinal strain is compelled to the negative values. Under compressive stress, in a tetragonal structure there is only 90° domain switching which may reduce the strain along the direction of the stress. Secondly, the strain vs. electric field hysteresis curve at zero stress shows the 180° domain switching. After the electric field is applied from zero to the maximum and then reduced to zero, the longitudinal strain remains the same value and the electric displacement remains opposite value. This property is the same as that of the 180° switching in tetragonal structure.

The stress dependence of the hysteresis loops seems to give some information about the laws governing the domain switching process. Some domain switching criteria are proposed below to explain experimental results. The piezoelectric equation for a domain is

$$\begin{aligned} \varepsilon &= \varepsilon^* + \boldsymbol{M}{:}\boldsymbol{\sigma} + \boldsymbol{E}\cdot\boldsymbol{d} \\ \boldsymbol{D} &= \boldsymbol{D}^* + \boldsymbol{d}{:}\boldsymbol{\sigma} + \boldsymbol{k}\cdot\boldsymbol{E} \end{aligned} \tag{3}$$

where $\boldsymbol{D}^*$ is the spontaneous electric displacement, ε^* the spontaneous strain, $\boldsymbol{M}$ the elastic compliance tensor, $\boldsymbol{d}$ the piezoelectric compliance tensor and $\boldsymbol{k}$ the dielectric permittivity. It is supposed that the temperature is constant. Thus the Gibbs' free energy, g, is a function of orientation tensor $\boldsymbol{R}$, stress $\boldsymbol{\sigma}$, electric field $\boldsymbol{E}$. According to the second thermodynamics law, a state with a higher Gibbs' energy tends to change to the state with a lower Gibbs' free energy. The difference of the Gibbs' energy of two states is the domain switching driving force. When the temperature is constant, the Gibbs' free energy can be expressed as

$$g = -\int_0^{\sigma} \varepsilon{:}\mathrm{d}\boldsymbol{\sigma} - \int_0^{E} \boldsymbol{D}\cdot\mathrm{d}\boldsymbol{E} \tag{4}$$

From Equations 3 and 4, we have

$$g = -\left(\varepsilon^*{:}\boldsymbol{\sigma} + \boldsymbol{D}^*\cdot\boldsymbol{E} + \tfrac{1}{2}\boldsymbol{\sigma}{:}\boldsymbol{M}{:}\boldsymbol{\sigma} + \tfrac{1}{2}\boldsymbol{E}\cdot\boldsymbol{k}\cdot\boldsymbol{E} + \boldsymbol{E}\cdot\boldsymbol{d}\cdot\boldsymbol{\sigma}\right) \tag{5}$$

At time t, the Gibbs' free energy is $g(\sigma_t,\ E_t)$. At time $t+\mathrm{d}t$, the Gibbs' free energy is $g(\sigma_{t+\mathrm{d}t},\ E_{t+\mathrm{d}t})$. Since there is energy dissipation associated with domain switching, the domain-switching driving force must be greater than a threshold denoted as W^{f} if domain switching occurs. Thus, the domain switching driven force, F, can be defined as

$$F(\sigma_{t+\mathrm{d}t},\ E_{t+\mathrm{d}t}) = \max\{g(\sigma_t,\ E_t) - g(\sigma_{t+\mathrm{d}t},\ E_{t+\mathrm{d}t})\} \tag{6}$$

For the 180° switching driven by an applied electric field parallel to the existing polarization such that E_3 is equal to or larger than E_{c}, the critical field, the spontaneous polarization switches from $+P^0$ to $-P^0$ where P^0 is the magnitude of the spontaneous polarization. Therefore, the criterion for ferroelectric switching of each grain under the applied electric field is defined on the basis of the work done in 180° polarization switching. When the work done on the system to remove the polarization from its current state plus the work done on the system to place the polarization in a new direction exceeds a critical value, the polarization will switch to the new direction. The criterion for the 180° polarization switching is thus

$$E_i\,\Delta P_i \geq W_{\mathrm{E}}^{\mathrm{f}} \tag{7}$$

where ΔP_i is the change of polarization. This change includes the loss of the amount P^0 from the prior orientation and the gain of the amount P^0 in one of the five possible new directions. According to Equation 6, the maximum driving force, $F_{\max}$, is $2P^0E$. When E equals the coercive electric field E_{c}, domain switching starts, and then we have

$$W_{\mathrm{E}}^{\mathrm{f}} = 2P^0E_{\mathrm{c}} \tag{8}$$

In terms of the micromechanics modeling [19], we have derived a formula to calculate P^0 as

$$P^r = \left[\frac{1}{4} + \frac{\sqrt{2}}{\pi}\left(\frac{\pi}{4} + \frac{1}{2}\right)\right]P^0 = 0.82P^0 \tag{9}$$

It is interesting to note that Baerwald [20] and Hwang *et al.* [15] gave a similar result as $P^r = 0.83P^0$. Using the measured values of P^r and E_{c} as listed in Table I, we can obtain the driven force of 180° domain switching.

The criterion for stress induced switching is that the mechanical work must equal or exceed a critical value, that is

$$\sigma_{ij}\,\Delta e_{ij} \geq W_{\mathrm{M}}^{\mathrm{f}} \tag{10}$$

where Δe_{ij} is the change in spontaneous strain. The change in spontaneous strain is zero for 180° switching and therefore only 90° switching is triggered by stress. Suppose that a stress is applied in the direction of the existing polarization that is alone the x_3 axis. According to Equation 6, the driving force is equal to

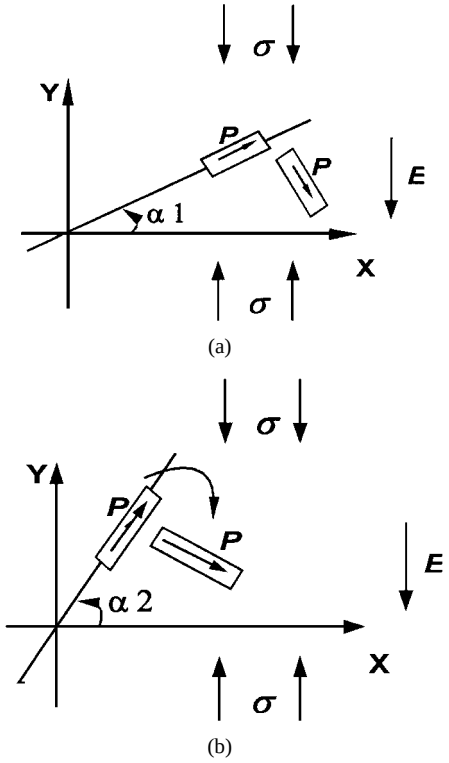

Figure 12 For 90° domain switching under combined mechanical and electrical loading: (a) the stress field impels the switching when $\alpha 1$ is less than 45°; and (b) the stress field hinders the switching when $\alpha 1$ is larger than 45°.

$(c - a/a_0)\sigma + 0.5(M_{1111} - M_{3333})\sigma$, where a_0, a and c are lattice constants of the cubic and tetragonal structures, respectively, and M_{1111} and M_{3333} are compliance constants in the directions of x_1 and x_3 axes. When the applied uniaxial stress, σ_{33}, equals the coercive value, σ_c, domain switching starts, and then we have

$$W_M^f = (c - a/a_0)\sigma_c + 0.5(M_{1111} - M_{3333})\sigma_c \quad (11)$$

The switching criterion for combined loading is met when the combined electrical and mechanical work exceeds a critical value. The direction of spontaneous polarization switches when the sum of the electrical and the mechanical work exceeds a critical value. From Equations 7 and 10, the combined switching criterion is given by

$$E_i \Delta P_i + \sigma_{ij} \Delta e_{ij} \geq W^f \quad (12)$$

where W^f is approximately equal to $2P^0 E_c$ [15]. Under the combined electrical and electrical loading, when the angle between the polarization direction and the direction of the applied compressive stress field is less than 45°, the change in spontaneous strain is negative for 90° domain switching as shown in Fig. 12a. Thus the stress field impels the domain switching. When the compressive stress becomes larger, this kind of domain switching may occur at a lower electrical field. Thus the coercive field is reduced as the applied compressive stress increases. On the other hand, when the angle between the polarization direction and the direction of the applied compressive stress field is larger than 45°, the change in spontaneous strain is positive for 90° domain switching as illustrated in Fig. 12b. Thus the stress field hinders the domain switching. When the compressive stress becomes larger, this kind of domain switching can only occur at a higher electrical field.

In short, because the compressive stress is just at the level that will cause 90° switching of favorably oriented grains, as soon as the electric field is applied, switching and straining of the ceramic commence. In this case the switching criteria of Equation 12 must be satisfied. However, Figs 7 and 8 indicate that a compressive stress can reduce the polarization and a large compressive stress can sweep the strain vs. electric field hysteresis loop, leading to the significant depolarization. For example, when $\sigma_{33} \geq 92$ MPa, the ceramic is nearly fully depolarized. Finally, from Equations 7–12, the differences in switching criteria for the electric-field driven switching and stress driven switching suggest that there may be a different energy barrier for the 90° and 180° switch. The energy of electric field driven switching is determined from a 180° switch whereas stress only involves a 90° switch. The difference may be accounted for by domain wall dynamics. Therefore, the main contribution to the hysteresis nonlinearity is the direct effect of polarization switching induced by either electric field or stress.

5. Conclusions

This paper presents the observed results of the electric-mechanical behaviors of the soft PZT-51 ceramic subjected to different electromechanical loads. A series of experiments show the electric displacement vs. electric field, the strain vs. electric field, and the strain vs. the stress exhibit linear behaviors under lower applied field and nonlinear behaviors under high applied field due to domain switching. Under combined electric-mechanical loads, a compressive stress can reduce the polarization, leading to the significant depolarization. That is, the electric-mechanical coupled behavior of the ferroelectric ceramic demonstrates that both the coercive field and the saturated field decrease as the compressive stress field increases. Furthermore, a sufficiently large compressive stress can even completely sweep the butterfly shaped strain vs. electric field hysteresis loop. The experimental results may further be understood by the proposed domain-switching criteria. Switching is the source of the classic butterfly shaped strain vs. electric field curve and the corresponding electric displacement vs. electric field curve. It is also the source of the nonlinear stress-strain curve. The differences in switching criteria for the electric field driven switching and stress driven switching suggest that there may be a different energy barrier for the 90° and 180° switch, which may be explained by domain wall dynamics. The results presented in this paper illustrate the importance of considering nonlinear electric-mechanical response when assessing a piezoelectric ceramic with a ferroelectric crystal for actuator application.

Acknowledgements

Support from the National Natural Science Foundation of China is gratefully acknowledged.

References

1. J. HERBERT, "Ferroelectric transducers and sensors" (Gordon and Breach, New York, 1982).
2. R. E. NEWNHAM, Q. C. XU, S. DUMAR and L. E. CROSS, *Smart Ceramics, Ferroelectrics* **102** (1990) 77–89.
3. I. CHOPRA, SPIE Proceedings, Bellingham, Washington, 1995.
4. B. JAFFE, W. R. COOK and H. JAFFE, "Piezoelectric Ceramics" (Academic Press, London and New York, 1971).
5. B. G. KOEPKE, K. D. MCHENRY, L. M. SEIFRIED and R. J. STOKES, in Proc. of IEEE Ultrasonic Symposium Williamsburg, Virginia, November 1986.
6. Y. E. PAK, *J. Appl. Mech.* **57** (1990) 647–653.
7. R. M. MCMEEKING, *J. Appl. Math. Phys.* **40** (1989) 615–627.
8. H. SOSA, *Int. J. Solid. Struct.* **28** (1989) 491–505.
9. Z. SUO, C. M. KUO, D. M. BARNET and J. R. WILLIS, *J. Mech. Phys. Solids* **40** (1992) 739–765.
10. S. B. PARK and C. T. SUN, *J. Amer. Ceram. Soc.* **78** (1995) 1475–1480.
11. T. ZHU and W. YANG, *Acta Mater.* **45** (1997) 4695–4702.
12. H. J. GAO, T. Y. ZHANG and P. TONG, *J. Mech. Phys. Solids* **45** (1997) 491–510.
13. H. CAO and A. EVANS, *J. Amer. Ceram. Soc.* **76** (1993) 890–896.
14. A. B. SCHAUFELE and K. H. HARDTL, *ibid.* **79** (1996) 2637–2640.
15. S. C. HWANG, C. S. LYNCH and R. M. MCMEEKING, *Acta Metall. Mater.* **43** (1995) 2073–2084.
16. C. S. LYNCH, *Acta Mater.* **44** (1996) 4137–4148.
17. X. CHEN, D. N. FANG and K. C. HWANG, *ibid.* **45** (1997) 3181–3189.
18. W. LU, D. N. FANG and K. C. HWANG, *Comput. Mater. Sci.* **8** (1997) 291–308.
19. *Idem., Key Eng. Mater.* **145–149** (1998) 983–988.
20. H.G. BAERWALD, *Phys. Rev.* **105** (1957) 480.

Received 28 July 1998
and accepted 11 February 1999